LETTER

Quantum annealing with manufactured spins

M. W. Johnson[1], M. H. S. Amin[1], S. Gildert[1], T. Lanting[1], F. Hamze[1], N. Dickson[1], R. Harris[1], A. J. Berkley[1], J. Johansson[2], P. Bunyk[1], E. M. Chapple[1], C. Enderud[1], J. P. Hilton[1], K. Karimi[1], E. Ladizinsky[1], N. Ladizinsky[1], T. Oh[1], I. Perminov[1], C. Rich[1], M. C. Thom[1], E. Tolkacheva[1], C. J. S. Truncik[3], S. Uchaikin[1], J. Wang[1], B. Wilson[1] & G. Rose[1]

Many interesting but practically intractable problems can be reduced to that of finding the ground state of a system of interacting spins; however, finding such a ground state remains computationally difficult[1]. It is believed that the ground state of some naturally occurring spin systems can be effectively attained through a process called quantum annealing[2,3]. If it could be harnessed, quantum annealing might improve on known methods for solving certain types of problem[4,5]. However, physical investigation of quantum annealing has been largely confined to microscopic spins in condensed-matter systems[6–12]. Here we use quantum annealing to find the ground state of an artificial Ising spin system comprising an array of eight superconducting flux quantum bits with programmable spin–spin couplings. We observe a clear signature of quantum annealing, distinguishable from classical thermal annealing through the temperature dependence of the time at which the system dynamics freezes. Our implementation can be configured *in situ* to realize a wide variety of different spin networks, each of which can be monitored as it moves towards a low-energy configuration[13,14]. This programmable artificial spin network bridges the gap between the theoretical study of ideal isolated spin networks and the experimental investigation of bulk magnetic samples. Moreover, with an increased number of spins, such a system may provide a practical physical means to implement a quantum algorithm, possibly allowing more-effective approaches to solving certain classes of hard combinatorial optimization problems.

Physically interesting in their own right, systems of interacting spins also have practical importance for quantum computation[15]. One widely studied example is the Ising spin model, where spins may take on one of two possible values: up or down along a preferred axis. Many seemingly unrelated yet important hard problems, in fields ranging from artificial intelligence[16] to zoology[17], can be reformulated as the problem of finding the lowest energy configuration, or ground state, of an Ising spin system.

Quantum annealing has been proposed as an effective way for finding such a ground state[2–5]. To implement a processor that uses quantum annealing to help solve difficult problems, we would need a programmable quantum spin system in which we could control individual spins and their couplings, perform quantum annealing and then determine the state of each spin. Until recently, physical investigation of quantum annealing has been confined to configurations achievable in condensed-matter systems, such as molecular nanomagnets[6–10] or bulk solids with quantum critical behaviour[11,12]. Unfortunately, these systems cannot be controlled or measured at the level of individual spins, and are typically investigated through the measurement of bulk properties. They are not programmable. Nuclear magnetic resonance techniques have been used to demonstrate a quantum annealing algorithm on three quantum spins[18]. Recently, three trapped ions were used to perform a quantum simulation of a small, frustrated Ising spin system[19].

One possible implementation of an artificial Ising spin system involves superconducting flux quantum bits[20–28] (qubits). We have

implemented such a spin system, interconnected as a bipartite graph, using an *in situ* reconfigurable array of coupled superconducting flux qubits[14]. The device fabrication is discussed in Methods and in Supplementary Information. The simplified schematic in Fig. 1a shows two superconducting loops in the qubit, each subject to an external flux bias Φ_{1x} or Φ_{2x}, respectively. The device dynamics can be modelled as a quantum mechanical double-well potential with respect to the flux, Φ_1, in loop 1 (Fig. 1b). The barrier height, δU, is controlled by Φ_{2x}. The energy difference between the two minima, $2h$, is controlled by Φ_{1x}. The two lowest energy states of the system, corresponding to clockwise or anticlockwise circulating current in loop 1, are labelled $|\downarrow\rangle$ and $|\uparrow\rangle$, with flux localized in the left- or the right-hand well (Fig. 1b), respectively. If we consider only these two states (a valid restriction at low temperature), the qubit dynamics is equivalent to those of an Ising spin, and we treat the qubits as such in what follows. Qubits (spins) are
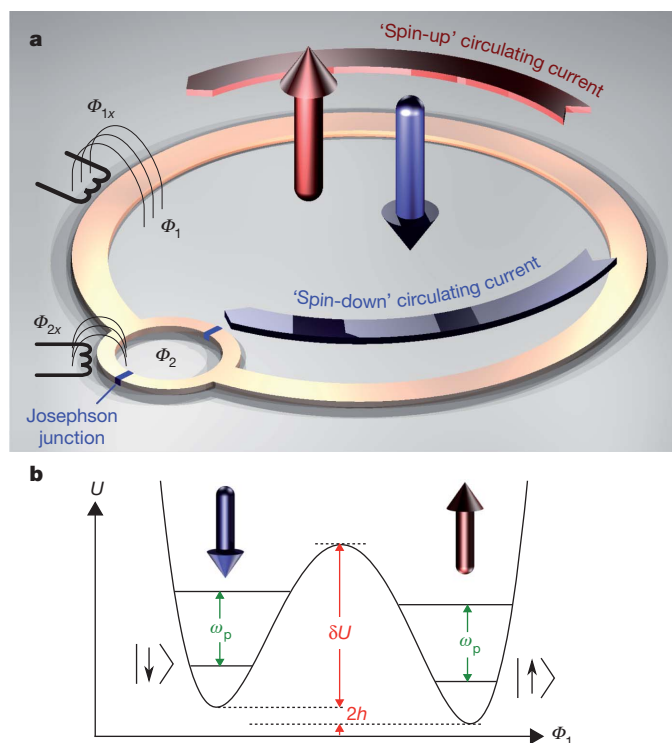

Figure 1 | Superconducting flux qubit. **a**, Simplified schematic of a superconducting flux qubit acting as a quantum mechanical spin. Circulating current in the qubit loop gives rise to a flux inside, encoding two distinct spin states that can exist in a superposition. **b**, Double-well potential energy diagram and the lowest quantum energy levels corresponding to the qubit. States $|\uparrow\rangle$ and $|\downarrow\rangle$ are the lowest two levels, respectively. The intra-well energy spacing is ω_p. The measurement detects magnetization, and does not distinguish between, say, $|\uparrow\rangle$ and excited states within the right-hand well. In practice, these excitations are exceedingly improbable at the time the state is measured.

[1]D-Wave Systems Inc., 100-4401 Still Creek Drive, Burnaby, British Columbia V5C 6G9, Canada. [2]Department of Natural Sciences, University of Agder, Post Box 422, NO-4604 Kristiansand, Norway. [3]Department of Physics, Simon Fraser University, Burnaby, British Columbia V5A 1S6, Canada.

coupled together using programmable coupling elements[29] which provide a spin–spin coupling energy that is continuously tunable between ferromagnetic and antiferromagnetic coupling. This allows spins to favour alignment or anti-alignment, respectively.

The behaviour of this system can be described with an Ising model Hamiltonian

$$\mathcal{H}_P = \sum_{i=1}^{N} h_i \sigma_i^z + \sum_{i,j=1}^{N} J_{ij} \sigma_i^z \sigma_j^z \qquad (1)$$

where for spin i σ_i^z is the Pauli spin matrix with eigenvectors $\{|\uparrow\rangle, |\downarrow\rangle\}$ and $2h_i$ is the energy bias; and $2J_{ij}$ is the coupling energy between the spins i and j. Our implementation allows each J_{ij} and h_i to be programmed independently within the constraints of the connectivity of our devices.

The quantum mechanical properties of the individual devices have been well characterized[13], but we are interested in what happens when several of them are coupled together. It is reasonable to ask whether this manufactured, macroscopic (~1 mm) system of artificial spins behaves quantum mechanically. We report here on an experiment that demonstrates a signature of quantum annealing in a coupled set of eight artificial Ising spins.

Whereas thermal annealing uses progressively weaker thermal fluctuations to allow a system to explore its energy landscape and arrive at a low-energy configuration, quantum annealing uses progressively weaker quantum fluctuations, mediated by tunnelling. In both thermal and quantum annealing, a system starts with a mixture of all possible states: a classical mixed state in the former and a coherent superposition in the latter.

Quantum annealing can be performed by slowly changing the system Hamiltonian

$$\mathcal{H}(t) = \Gamma(t) \sum_{i=1}^{N} \Delta_i \sigma_i^x + \Lambda(t) \mathcal{H}_P$$

where Γ decreases from one to zero and Λ increases from zero to one monotonically with time, and Δ_i parameterizes quantum mechanical tunnelling between $|\uparrow\rangle$ and $|\downarrow\rangle$.

At the beginning of the annealing, $\Gamma = 1$, $\Lambda = 0$ and the system is fully characterized by the transverse terms, $\sum_{i=1}^{N} \Delta_i \sigma_i^x$. The ground state of this is a superposition of all states in the σ_z basis. It is straightforward to initialize the system in this state. During quantum annealing, the transverse term is gradually turned off ($\Gamma \rightarrow 0$) and the weight of the Ising Hamiltonian, $\mathcal{H}_P$, is increased ($\Lambda \rightarrow 1$) (Fig. 2b). If this annealing is done slowly enough, the system should remain in the ground state at all times, thus ending up in the ground state of $\mathcal{H}_P$ (ref. 4).

The above description of quantum annealing is in the language of an ideal Ising spin system. Let us look more closely at what this means for an individual flux qubit. During annealing, the energy barrier, $\delta U(t)$, between the two wells is gradually raised (Fig. 2a). If thermal fluctuations are dominant, then the qubit dynamics may be viewed as thermal activation over the barrier with a rate that is proportional to $e^{-\delta U/k_B T}$ at a temperature T (k_B, Boltzmann's constant). This suggests that the dynamics stops when $\delta U \gg k_B T$. Because δU is increasing with time, this freezing out happens at $t \approx t_{\text{freeze}}^{\text{TA}}$, where $\delta U(t_{\text{freeze}}^{\text{TA}}) \approx k_B T$. Within the relevant regime, δU is nearly linear in time, therefore classically we expect $t_{\text{freeze}}^{\text{TA}}$ to be linearly dependent on T.

If, however, the dominant fluctuations are quantum mechanical, then the qubit may tunnel between the two wells, that is, between states $|\downarrow\rangle$ and $|\uparrow\rangle$. Raising the barrier, by increasing δU, reduces this tunnelling until at some point it becomes negligible. In this picture, we expect to find a quantum freeze-out time, $t_{\text{freeze}}^{\text{QA}}$, that is independent of (or at least very weakly dependent on) T. By measuring the T dependence of t_{freeze}, the time at which the system can no longer respond to changes in its energy landscape, we can determine whether classical thermal
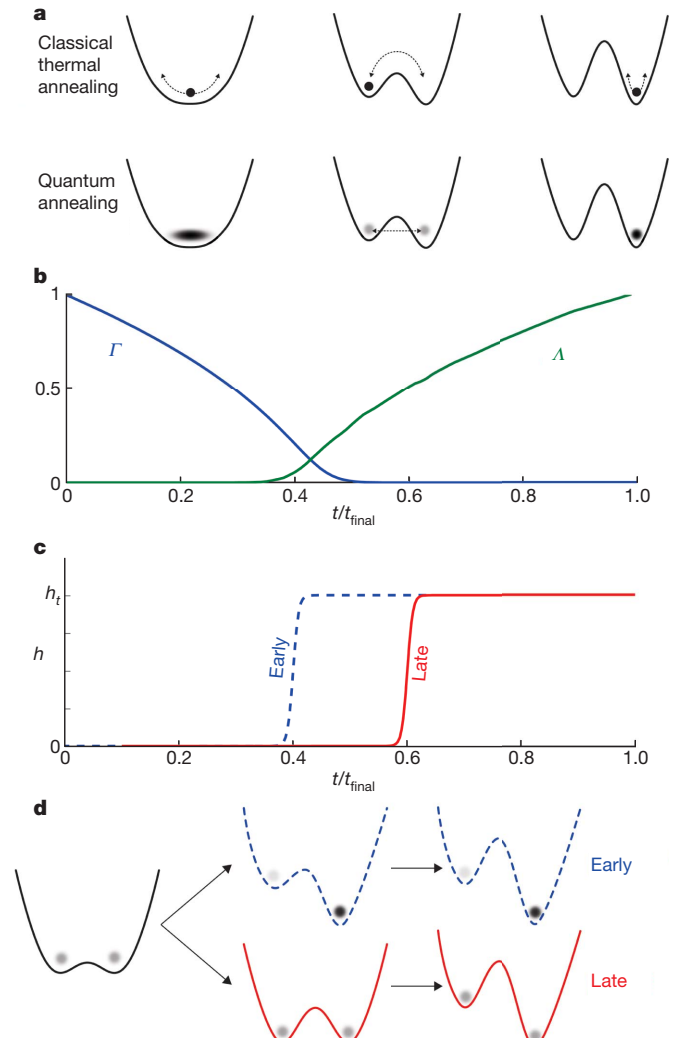

Figure 2 | Quantum annealing. a, Annealing is performed by gradually raising the energy barrier between states. In thermal annealing, when the barrier becomes much larger than $k_B T$ thermal excitation over the barrier eventually ceases, at some time $t_{\text{freeze}}^{\text{TA}}$. In quantum annealing, tunnelling between states also will eventually cease, at a time $t_{\text{freeze}}^{\text{QA}}$. **b**, The value of the parameters Γ and Λ during annealing are not independent of each other in the flux qubit. The annealing ends at $t_{\text{final}} = 148\,\mu s$. **c**, Changing the value of $h(t)$ (see **d**) at various points during annealing can be used to probe the freeze-out time, t_{freeze}. **d**, Double-well potential during annealing. If h is turned on early enough (blue line), the system follows the ground state through annealing and reaches the final ground state of equation (1) with high probability. If $h(t)$ is turned on too late (red line), the state probabilities are determined by the earlier Hamiltonian, for which $h = 0$.

activation or quantum tunnelling is the dominant effect governing qubit dynamics.

Here we modify this annealing procedure to perform a specialized experiment that permits us to distinguish between these two cases, by allowing the h_i in equation (1) to be time dependent. We measure the 'step response' of the system to rapid changes in h (rapid by comparison with changes in Γ and Λ) at different stages during the annealing process. In this way, we are able to measure t_{freeze}. By measuring t_{freeze} as a function of T, we can infer whether the system dynamics is dominated by thermal or quantum fluctuations.

We abruptly increase h from zero to a level h_t at a delay time t_d during annealing as shown in Fig. 2c, and then measure the probability of the spin being in either configuration at the end of annealing. If h is switched on very early in the annealing process, while the barrier δU is still small in comparison with the thermal or quantum transition

energy scales, then the qubit will quickly respond and will be able to evolve into the lower energy well, such that $P_\uparrow$, the probability of the spin being in state $|\uparrow\rangle$, is greater than 1/2. The value of $P_\uparrow$ will depend on both h_t and T, as the system will strive to achieve a Boltzmann distribution of its population statistics between $|\downarrow\rangle$ and $|\uparrow\rangle$. However, if h is not turned on until after the barrier has been raised sufficiently high ($t_d > t_{freeze}$), the system will not be able to follow it and will be equally likely to settle into either potential energy well, such that $P_\uparrow \approx 1/2$. These two situations are illustrated in Fig. 2d. For intermediate values of t_d, the qubit will only partly succeed in responding to the sudden application of the bias h.

Example plots of measured $P_\uparrow$ values versus t_d for a single qubit at different temperatures are shown in Fig. 3a. In this case, $h_t = 2.55 \pm 0.04$ GHz and $\Delta = 9.0 \pm 0.2$ GHz. Experimental parameters controlling the annealing process are discussed in Supplementary Information. As expected, $P_\uparrow$ shows an initial ($t_d \approx 0$) T dependence and then converges to 1/2 at late delay times. These curves were numerically fitted to extract t_{freeze}, the time at the middle of this transition region, which in turn is plotted versus T in Fig. 3b. The curve used for the fitting was obtained by numerical simulations of this
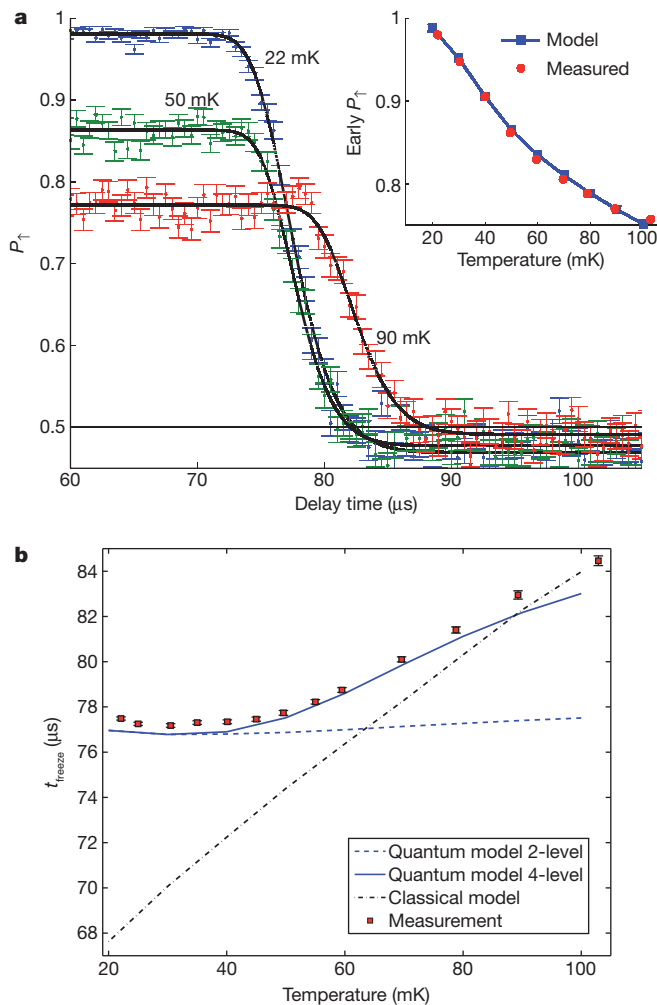
process using a quantum mechanical model as discussed in the Supplementary Information.

In addition to the experimental results, in Fig. 3b we show the results of three different numerical simulations. In all three cases, the model parameters were independently measured for the individual devices, leaving no free parameters. A simulation, based on a classical model, treated the flux in the two superconducting loops as the coordinates of a discrete particle inside the two-dimensional flux qubit potential, and then coupled that particle to a thermal bath. The dynamics was simulated by numerically solving the Langevin equation, as described in Supplementary Information. The classically simulated t_{freeze} value varies linearly with T, as expected. The other two simulations involved solving a quantum mechanical model of a flux qubit coupled to a thermal bath in which only the two or, respectively, four lowest-lying energy levels of the flux qubit were kept. The dynamics was simulated by numerically solving a non-Markovian density matrix equation of motion (Supplementary Information). These two models will be referred to here as the two-level and four-level quantum models.

The experimental results clearly show a saturation of t_{freeze} below 45 mK, in agreement with both the two-level and the four-level quantum models and in disagreement with the classical model. The experimental data deviate from the two-level model above 45 mK, as the upper energy levels in the flux qubit start to become thermally occupied. The four-level quantum model describes the behaviour of the system well up to 80 mK, where more energy levels start to be occupied. The experimental data asymptotically approach the classical simulation results at higher temperatures. We propose that if the quantum mechanical modelling were extended by keeping even more energy levels, then it would reproduce the data to ever higher temperatures.

Both the measured and the simulated (four-level quantum model) T dependence of $P_\uparrow$ for $t_d \approx 0$ are shown in the inset of Fig. 3a. Because this probability has a strong T dependence for $t_d < t_{freeze}$, its measurement provides us with an independent check on the effective temperature of the spin system in this regime. Moreover, because the probability does not saturate at 45 mK, where t_{freeze} saturates, it is a clear indication that saturation of t_{freeze} is not a result of saturation of qubit temperature. The key conclusion we draw from Fig. 3b is that our qubit dynamics is best characterized as being quantum mechanical in nature for $T \lesssim 80$ mK. The system evolves to its ground state through a process of quantum annealing. But so far we have shown this only for an individual qubit. It remains to be shown whether quantum annealing can be performed on several spins coupled together.

To investigate this, we now configure our array into a chain of eight ferromagnetically coupled artificial spins (Fig. 4), with $J_{i,i+1} = -J$ for $i = 1, 2, \ldots, 7$ along the chain and $J_{ij} = 0$ otherwise. In our experiment, we used $J = 12.78$ GHz, which is near the maximum available for the couplers. The lowest-energy configurations of this system correspond to the two ferromagnetic states $|\uparrow\uparrow\uparrow\uparrow\uparrow\uparrow\uparrow\uparrow\rangle$ and $|\downarrow\downarrow\downarrow\downarrow\downarrow\downarrow\downarrow\downarrow\rangle$. Applying strong but opposing biases, $h_B = \pm 2J$, to the ends of the chain introduces frustration into the system, and the lowest-energy configuration will have a break in the ferromagnetic order; this is known as a domain wall (where the spins change direction). For example, we depict the state $|\uparrow\uparrow\uparrow\uparrow\downarrow\downarrow\downarrow\downarrow\rangle$ in Fig. 4a, for which the domain wall is the middle of the chain.

In our step response experiment with the spins configured as a chain, all six spins internal to the chain begin annealing with $h = 0$. In this situation, it is energetically equivalent for the domain wall to be between any adjacent pair of spins, and each such state should occur with probability $P = 1/7$. If we leave $h = 0$ for too long ($t_d \gg t_{freeze}$), we expect to observe this distribution of single-domain-wall states. At $t = t_d$, we apply a uniform bias, $h_t = 0.1J$, to the six intermediate spins. Now the ground state is $|\uparrow\uparrow\uparrow\uparrow\uparrow\uparrow\uparrow\downarrow\rangle$, with the domain wall at the right-hand end of Fig. 4b. More system energy is required for the domain wall to occupy positions to the left in Fig. 4. If $t_d \ll t_{freeze}$, we should observe state $|\uparrow\uparrow\uparrow\uparrow\uparrow\uparrow\uparrow\downarrow\rangle$ occurring with probability $P > 1/7$. As in the single-qubit case, we measure t_{freeze} by finding the transition point

Figure 3 | Single-qubit results. a, Measured final ground-state probability, $P_\uparrow$, in a single qubit versus the delay time, t_d, of a step $h_t = 2.55 \pm 0.04$ GHz in energy bias, for $T = 22$ mK (blue), 50 mK (green) and 90 mK (red). The solid lines are the result of fits used to extract the freeze-out time, t_{freeze}. Inset, measured and simulated (four-level quantum model) T dependence of $P_\uparrow$ for $t_d \approx 0$. **b**, Measured t_{freeze} versus T (red points). We also show simulated plots of t_{freeze} from two-level (dashed blue) and four-level (solid blue) quantum mechanical models and from a classical model of the qubit (black). Error bars, 1σ s.e.
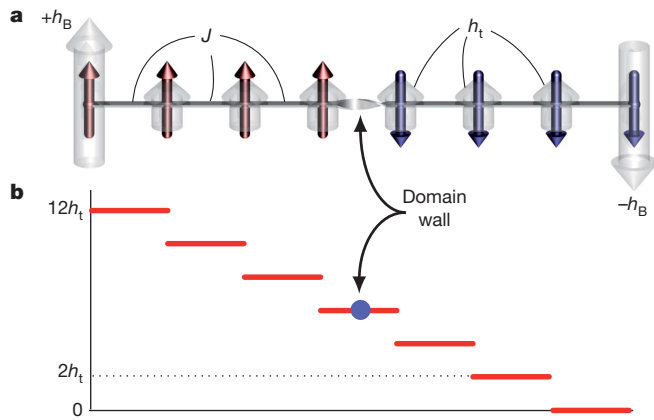
Figure 4 | Eight-qubit ferromagnetic chain. a, Chain of eight ferromagnetically coupled qubits with uniform coupling coefficient $J_{i,i+1} = -J < 0$ for $i = 1, 2, …,$ 7. The two end qubits are biased in opposite directions with $h_B = \pm 2J$, such that a domain wall has to form within the chain. All middle qubits are biased with a target $h_t = 0.1J$. The configuration depicted is an excited state. The faint grey arrows indicate the spin biases h_i. **b**, Effective energy of the spin state corresponding to there being a domain wall at each position along the chain at finite h_t. The ground state is the rightmost site.

between these two state distributions (Fig. 5a). As before, we are able to determine the dominant mechanism (thermal or quantum annealing) by measuring the T dependence of t_{freeze}.

A summary of the experimental results for the eight-qubit chain is shown in Fig. 5b. As with the single-qubit case, the experimentally determined t_{freeze} values show saturation at low T and a crossover to near-linear T dependence for $T \gtrsim 45$ mK. In this case, the classical model treats the fluxes of all eight qubits as coordinates of a discrete particle in a sixteen-dimensional potential. The classical model does not capture the behaviour observed at low T. However, the quantum models quantitatively agree with the experimental results for $T \lesssim 50$ mK. At higher temperatures, the classical model and the four-level quantum model are both in qualitative agreement with the experimental results.

The saturation of t_{freeze} at low T for the single-spin and eight-spin systems is a clear signature of quantum annealing. It cannot be explained by an experimental failure to reach lower T, as $P_{\uparrow\uparrow\uparrow\uparrow\uparrow\uparrow\uparrow\downarrow}$, for $t_d \ll t_{freeze}$, follows its expected temperature dependence at low T (Fig. 5a, inset). Nor can it be explained by classical thermal activation processes, because for these lowering T would always decrease the rate of thermal activation. This means that, classically, freeze-out should happen earlier in the evolution, where the barrier is smaller, that is, saturation is not possible. This qualitative argument is independent of the detailed model used to describe classical dynamics. The low-temperature behaviour of t_{freeze} in this system of eight coupled artificial spins cannot be explained by thermal activation but is naturally explained by quantum tunnelling. This measurement and its result are reminiscent of the T-dependent escape rate measurements in the pioneering works on macroscopic quantum tunnelling[30,31], which demonstrated a clear signature of quantum tunnelling in current-biased Josephson junctions.

This brings us to our main conclusion: a programmable artificial spin system manufactured as an integrated circuit can be used to implement a quantum algorithm. The experiments presented here constitute a step between understanding single-qubit annealing and understanding the multi-qubit processes that could be used to find low-energy configurations in a realistic adiabatic quantum processor. In addition to its problem-solving potential, a system such as this also provides an interesting test bed for investigating the physics of inter-acting quantum spins, and is an important step in an ongoing investigation into much more complex spin systems realized using this type of architecture. Although our manufactured spin system is not yet a
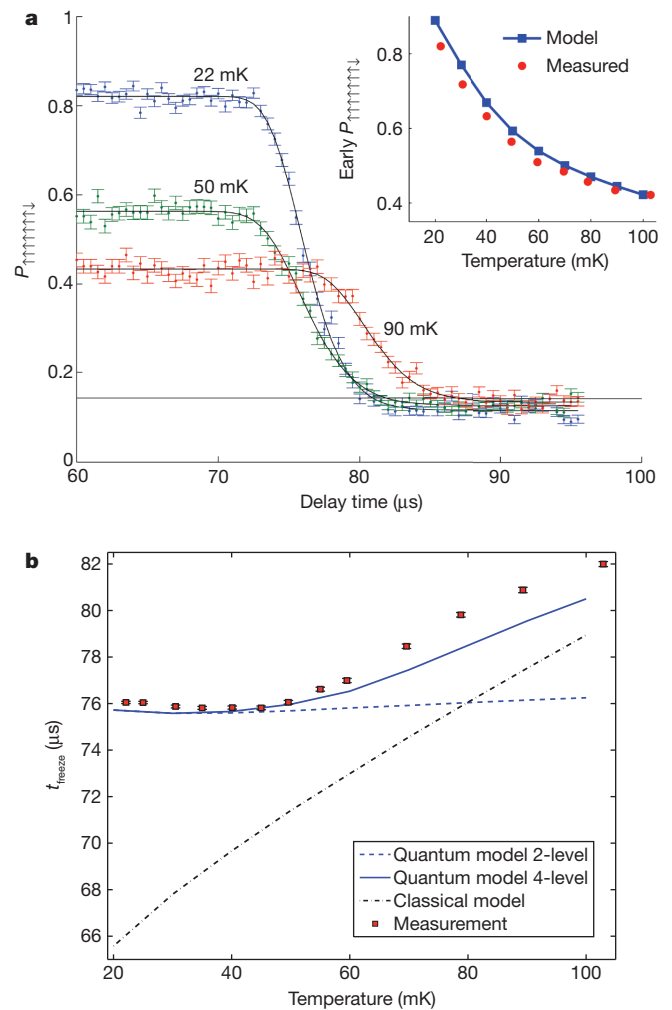

Figure 5 | Results for the eight-qubit ferromagnetic chain. a, Measured final ground-state probability, $P_{\uparrow\uparrow\uparrow\uparrow\uparrow\uparrow\uparrow\downarrow}$, in the eight-qubit chain versus t_d for $h_t = 0.1J$ and $T = 22$ mK (blue), 50 mK (green) and 90 mK (red). The solid lines are the result of fits used to extract the freeze-out time, t_{freeze}. Inset, measured and simulated (four-level quantum model) T dependence of $P_{\uparrow\uparrow\uparrow\uparrow\uparrow\uparrow\uparrow\uparrow}$ for $t_d \approx 0$. **b**, Measured t_{freeze} versus T (red points). We also show simulated plots of t_{freeze} from two-level (dashed blue) and four-level (solid blue) quantum mechanical models and from a classical model of the qubits (black). Error bars, 1σ s.e.

universal quantum computer[15], by adding a new type of coupler between the qubits, universal quantum computation would become possible[32].

METHODS SUMMARY

Sample fabrication. We fabricated samples in a four-niobium-layer superconducting integrated circuit process using a standard Nb/AlO$_x$/Nb trilayer, a TiPt resistor layer and planarized SiO$_2$ dielectric layers applied by plasma-enhanced chemical vapour deposition. Design rules included 0.25-μm lines and spaces for wiring layers and a minimum junction diameter of 0.6 μm. Circuit details are discussed in ref. 13.

Thermometry. We measured the effective device temperature attained during these experiments in two ways. The first is based on analysis of the single-qubit macroscopic resonant tunnelling. The second is based on measurement of $P_\uparrow$ versus Φ_{1x} at equilibrium and at a fixed barrier height. Both methods are described in ref. 33 and in Supplementary Information. Both measurements generally agreed with the ruthenium oxide thermometer on the dilution refrigerator mixing chamber to within a few millikelvin over the range of temperatures used in the experiment.

Confirmation of the thermometry comes from the agreement between the measured T dependence of $P_\uparrow(t_d \ll t_{freeze})$ and that predicted by the four-level quantum model (insets of Fig. 3a and Fig. 5a). This is discussed further in Supplementary Information.

Annealing. Annealing was performed by sweeping Φ_{2x} (Fig. 1b) from $0.592\Phi_0$ to $0.652\Phi_0$ linearly over a period of 148 μs, where Φ_0 is the magnetic flux quantum. These values bracket the point at which the qubit becomes bistable. The devices used are those analysed in ref. 14. (See Supplementary Information for more details.)

1. Barahona, F. On the computational complexity of Ising spin glass models. *J. Phys. Math. Gen.* **15**, 3241–3253 (1982).
2. Kadowaki, T. & Nishimori, H. Quantum annealing in the transverse Ising model. *Phys. Rev. E* **58**, 5355–5363 (1998).
3. Finnila, A. B., Gomez, M. A., Sebenik, C., Stenson, C. & Doll, J. D. Quantum annealing: a new method for minimizing multidimensional functions. *Chem. Phys. Lett.* **219**, 343–348 (1994).
4. Farhi, E. *et al.* A quantum adiabatic evolution algorithm applied to random instances of an NP-complete problem. *Science* **292**, 472–475 (2001).
5. Hogg, T. Quantum search heuristics. *Phys. Rev. A* **61**, 052311 (2000).
6. Wernsdorfer, W. Molecular nanomagnets: towards molecular spintronics. *Int. J. Nanotechnol.* **7**, 497–522 (2010).
7. Carretta, S., Liviotti, E., Magnani, N., Santini, P. & Amoretti, G. S mixing and quantum tunneling of the magnetization in molecular nanomagnets. *Phys. Rev. Lett.* **92**, 207205 (2004).
8. Caciuffo, R. *et al.* Spin dynamics of heterometallic Cr_7M wheels (M = Mn, Zn, Ni) probed by inelastic neutron scattering. *Phys. Rev. B* **71**, 174407 (2005).
9. Guidi, T. *et al.* Inelastic neutron scattering study of the molecular grid nanomagnet Mn-[3 × 3]. *Phys. Rev. B* **69**, 104432 (2004).
10. Waldmann, O., Guidi, T., Carretta, S., Mondelli, C. & Dearden, A. L. Elementary excitations in the cyclic molecular nanomagnet Cr_8. *Phys. Rev. Lett.* **91**, 237202 (2003).
11. Brooke, J., Bitko, D., Rosenbaum, T. F. & Aeppli, G. Quantum annealing of a disordered magnet. *Science* **284**, 779–781 (1999).
12. Ghosh, S. & Rosenbaum, T. F. Aeppli, G. & Coppersmith, S. N. Entangled quantum state of magnetic dipoles. *Nature* **425**, 48–51 (2003).
13. Harris, R. *et al.* Experimental demonstration of a robust and scalable flux qubit. *Phys. Rev. B* **81**, 134510 (2010).
14. Harris, R. *et al.* Experimental investigation of an eight-qubit unit cell in a superconducting optimization processor. *Phys. Rev. B* **82**, 024511 (2010).
15. Aharonov, D. *et al.* Adiabatic quantum computation is equivalent to standard quantum computation. *SIAM J. Comput.* **37**, 166–194 (2007).
16. Hinton, G. E. & Salakhutdinov, R. R. Reducing the dimensionality of data with neural networks. *Science* **313**, 504–507 (2006).
17. Chen, X. & Tompa, M. Comparative assessment of methods for aligning multiple genome sequences. *Nature Biotechnol.* **28**, 567–572 (2010).
18. Steffen, M., van Dam, W., Hogg, T., Breyta, G. & Chuang, I. Experimental implementation of an adiabatic quantum optimization algorithm. *Phys. Rev. Lett.* **90**, 067903 (2003).
19. Kim, K. *et al.* Quantum simulation of frustrated Ising spins with trapped ions. *Nature* **465**, 590–593 (2010).
20. Lupaşcu, A. *et al.* Quantum non-demolition measurement of a superconducting two-level system. *Nature Phys.* **3**, 119–125 (2007).
21. Berns, D. M. *et al.* Amplitude spectroscopy of a solid-state artificial atom. *Nature* **455**, 51–58 (2008).
22. Poletto, S. *et al.* Coherent oscillations in a superconducting tunable flux qubit manipulated without microwaves. *N. J. Phys.* **11**, 013009 (2009).
23. DiCarlo, L. *et al.* Demonstration of two-qubit algorithms with a superconducting quantum processor. *Nature* **460**, 240–244 (2009).
24. Bennett, D. A. *et al.* Decoherence in rf SQUID qubits. *Quantum Inf. Process.* **8**, 217–243 (2009).
25. Yoshihara, F., Nakamura, Y. & Tsai, J. S. Correlated flux noise and decoherence in two inductively coupled flux qubits. *Phys. Rev. B* **81**, 132502 (2010).
26. Il'ichev, E. *et al.* Multiphoton excitations and inverse population in a system of two flux qubits. *Phys. Rev. B* **81**, 012506 (2010).
27. Vion, D. *et al.* Manipulating the quantum state of an electrical circuit. *Science* **296**, 886–889 (2002).
28. Burkard, G., Koch, R. H. & DiVincenzo, D. P. Multilevel quantum description of decoherence in superconducting qubits. *Phys. Rev. B* **69**, 064503 (2004).
29. Harris, R. *et al.* Compound Josephson-junction coupler for flux qubits with minimal crosstalk. *Phys. Rev. B* **80**, 052506 (2009).
30. Voss, R. F. & Webb, R. A. Macroscopic quantum tunneling in 1-μm Nb Josephson junctions. *Phys. Rev. Lett.* **47**, 265–268 (1981).
31. Devoret, M. H., Martinis, J. M. & Clarke, J. Measurements of macroscopic quantum tunneling out of the zero-voltage state of a current-biased josephson junction. *Phys. Rev. Lett.* **55**, 1908–1911 (1985).
32. Biamonte, J. D. & Love, P. J. Realizable Hamiltonians for universal adiabatic quantum computers. *Phys. Rev. A* **78**, 012352 (2008).
33. Harris, R. *et al.* Probing noise in flux qubits via macroscopic resonant tunneling. *Phys. Rev. Lett.* **101**, 117003 (2008).

Author Contributions M.H.S.A. and M.W.J. developed the idea for the experiment; M.W.J. conducted the experiment; T.L., R.H., M.W.J. and J.W. conducted supporting experiments; M.H.S.A. developed the theory; N.D., F.H. and M.H.S.A. developed simulation code; N.D., M.H.S.A., M.W.J., F.H. and C.J.S.T. performed simulations and analysed results; M.W.J., M.H.S.A., S.G. and R.H. wrote the article; M.W.J., S.G., M.H.S.A. and N.D. generated the figures; A.J.B., R.H., J.J., M.W.J., T.L., I.P., E.M.C. and B.W. developed measurement algorithms and testing software; C.R., S.U. and M.C.T. achieved the low-magnetic-field environment for the device; C.E. and C.R. mounted the sample, P.B., E.T., A.J.B., R.H., J.J., M.W.J. and T.L. designed the devices; E.L., N.L. and T.O. fabricated the devices; M.C.T. and S.U. developed the testing apparatus; K.K. allowed use of BOINC for classical simulations; J.P.H. and G.R. provided logistical support; and J.P.H. selected the chip.